

# Interplay of the emission from thermal and direct sources in relativistic heavy ion collisions\*

Piotr Bożek<sup>1,2,†</sup>

<sup>1</sup>*Institute of Physics, Rzeszów University, PL-35959 Rzeszów, Poland*

<sup>2</sup>*The H. Niewodniczański Institute of Nuclear Physics, PL-31342 Kraków, Poland*

The separation of the source created in ultrarelativistic heavy-ion collisions into a thermalized dense core and an outer mantle consisting of independent nucleon-nucleon collisions is discussed. Evidence for such a two component picture is found in transverse mass spectra of kaon, protons and antiprotons produced in Au-Au collisions at  $\sqrt{s} = 200\text{GeV}$ . Estimates of the sizes of the thermal and direct sources are compared to models separating the interaction zone into a core and a corona, according to the density of participants or to the number of collisions. Consequences for the modeling of the dynamics of the small size, thermalized core are described. New initial conditions corresponding to the dense core lead to a stronger azimuthal asymmetry of the hydrodynamically expanding fireball, pressure gradients also increase. 2+1-dimensional hydrodynamic simulations are presented starting from all the matter in the interaction region or from the dense, thermal part of the source. We find faster transverse expansion and stronger elliptic flow for dense core initial conditions. For different impact parameters we find very similar spectra of the thermal part of the source and only adding particles emitted directly from nucleon-nucleon collisions in the corona the experimentally observed softening of the spectra with increasing impact parameter is reproduced. The elliptic flow is stronger for particles emitted from a source separated into a core and a corona.

PACS numbers: 25.75.-q, 25.75.Dw, 25.75.Ld

Keywords: relativistic heavy-ion collisions, Glauber model, hydrodynamic model, collective flow

## I. INTRODUCTION

A vast number of experimental observations indicate that matter created in relativistic heavy ion collisions is a strongly interacting, dense and thermalized medium [1, 2, 3, 4]. Transverse momentum spectra of emitted particles are thermal. Fitted temperatures are in the range of 100 – 160 MeV and the transverse velocity of the emitting source is 0.5 – 0.6c on average. The presence of a substantial transverse flow confirms the formation of a dense matter that expands collectively. Since no transverse flow is present in the initial stage of the collision, the observed expansion results from a build up of collective flow from density gradients in the fireball. The expansion continues until particles decouple from the system, i.e. until freeze-out. Another important achievement is the experimental observation of azimuthal asymmetry in the collective flow. Spectra of particles emitted at central rapidities are written using the elliptic flow coefficient  $v_2$ ,

$$\frac{dN}{p_\perp dp_\perp d\phi} = \frac{dN}{2\pi p_\perp dp_\perp} (1 + v_2(p_\perp) \cos(2\phi)). \quad (1.1)$$

The parameter  $v_2$  has been measured for a variety of identified particles and transverse momenta. For non-central collisions substantial elliptic flow is observed, increasing with transverse momenta up to  $p_\perp \simeq 1.5\text{GeV}$ . The azimuthal asymmetry in this kinematical range

can be explained by the collective expansion of an azimuthally asymmetric source followed by thermal emission at freeze-out. Hanbury Brown-Twiss (HBT) correlations between identical particles allow to estimate the lifetime and the size of the fireball. Correlation analysis confirms the existence of a strong collective flow and suggest a fast expansion of the system.

Thermal fits [5] of spectra of emitted particles show an increase of the radial flow with centrality and a decrease of the temperature [6]. The effect manifest itself as well as an increase of the average  $p_\perp$  of emitted particles with centrality. Observed ratios of the number of produced particles can be calculated assuming particle production in a state of chemical equilibrium, defined by the temperature and the values of chemical potentials [7, 8, 9, 10, 11]. For central collisions at  $\sqrt{s} = 200\text{GeV}$  particle ratios follow chemical equilibrium, but when going to more peripheral collisions the relative number of strange particles produced decreases. This decrease is taken into account by the introduction of a strangeness suppression factor  $\lambda_s \leq 1$  that reaches 1 for central collisions.

Properties of the hot, dense and strongly interacting fireball can be modelled by relativistic fluid dynamics (for reviews see [12, 13, 14, 15]). Matter is usually assumed to be a perfect fluid, although possible effects of viscosity and other sources of dissipation are discussed. Hydrodynamic models qualitatively describe the dynamics of the hot source created in the collision. Fluid dynamic models include several parameters and assumptions: initial starting time and initial density profile, the equation of state (EOS), the freeze-out conditions and sometimes shear viscosity. Only recently a consistent description

\*Supported by Polish Ministry of Science and Higher Education under grant N202 034 32/0918

†Electronic address: Piotr.Bozek@ifj.edu.pl

of soft observables measured in heavy ion collisions at RHIC energies has been achieved [16, 17, 18]. Assuming an early thermalization and an EOS without a soft-point, transverse momentum spectra, elliptic flow, HBT radii, and azimuthally sensitive HBT radii could be described in central and semi-peripheral collisions. The dependence of the elliptic flow on the impact parameter and in particular its scaling properties [19] indicate that an almost perfect fluid is formed with possible deviations due to dissipative effects in most peripheral collisions.

The dependence of strangeness production, average  $p_{\perp}$ , spectra, transverse and elliptic flows on centrality is due to a change of the size and shape of the fireball. To explain the observed systematics one has to invoke different freeze-out conditions for collision events in different centrality classes. While some reduction of the transverse flow with the decreasing size of the system is possible, a significant change in the freeze-out temperature is not understood. However, recently the effect of energy and momentum conservation on the fitted temperatures has been noticed [20]. The reduced strangeness production in peripheral collisions calls for the introduction of a new parameter, the strangeness suppression factor, describing the degree to which chemical equilibration is achieved. On the other hand, a simple idea assuming that the interaction zone in heavy-ion collisions is composed of two sources explains the observed impact-parameter dependence [21]. The most dense part of the interaction zone is the thermal fireball, that behaves collectively and is chemically and thermally equilibrated. The outer mantle of the interaction zone does not take part in the fireball formation. Particles emitted from this part of the system do not reinteract significantly and their spectra and abundances are the same as in nucleon-nucleon (N-N) collisions. Assuming a minimal density of participant nucleons in the transverse plane necessary for the local thermalization [21], we could reproduce the centrality dependence of the multiplicity of charged particles and of the strange particle suppression ( $K/\pi$  ratio) on centrality. The thermal source emits more particle per participant nucleon pair than a single N-N collision. In the most central collisions 95% of the participant nucleons end up in the thermal fireball and only 5% of them are in the corona, on the other hand for centralities 70-80% the corona dominates the emission. The change in the proportion of the thermal fireball and of the corona with centrality leads to a stronger than linear increase of the particle multiplicity with the number of participants. A very similar mechanism can explain the change in the ratio of strange particles to other particles with the centrality of the collision. We assume that the thermal fireball is always close to a complete chemical equilibrium, but its proportion in the total particle emission goes down in peripheral collisions, as relatively more particles are emitted from the outer mantle. The rate of the emission of strange particles from the corona is below chemical equilibrium. The assumption [22] that jet absorption is stronger in the dense thermal fireball leads to results con-

sistent with the experimental data on nuclear attenuation rate [21]. It has been noticed that the spectra of particles emitted from the two components in the interaction region have different slopes [23]. For central collisions, with increasing proportion of particles emitted from the thermal fireball, the spectra become harder. Recently, Baccattini and Manninen [24] analyzed strangeness suppression in peripheral nuclear collisions for different particle species assuming a two component source. They used a different definition of the thermalized fireball based on the number of collisions that a participant undergoes.

In the present work we analyze the two-component picture of the interaction zone and its consequences on the spectra and elliptic flow of emitted particles. In Sect. II we perform a fit of the thermal core and corona sizes for different centralities in order to reproduce the observed spectra of kaons, protons and antiprotons. We compare the extracted thermal fireball and corona sizes for different centralities with models dividing the interaction region according to the density of participants in the transverse plane [21] or according to the number of collisions [24]. In Sect. III we look at the geometry of the thermal fireball for different impact parameters, and compare it to the geometry of the fireball calculated in the usual Glauber model. Then in Sect. IV a hydrodynamic evolution of the thermal fireball is performed ending with a freeze-out emission of particles. Calculated spectra and elliptic flow are compared to results of a hydrodynamic expansion starting from a fireball consisting of the whole interaction region. We find that spectra of particles emitted from an expanding thermal, dense fireball are harder and show a stronger elliptic flow, than standard hydrodynamic model predictions. The differences get partially reduced when emission from the corona is added to the final spectra.

## II. TWO COMPONENTS IN THE SPECTRA

Experimental data on identified particle spectra at different impact parameters show a hardening of the spectra in transverse momentum when going to central collisions. The effect is more pronounced for heavy particles, which indicates the role of the transverse flow therein. In the two-component model of the emission, particles originate from two different zones, the thermal fireball and the outer corona. The dominant reason for the change of the spectra with centrality is not the change of the parameters of the thermal source (freeze-out temperature and velocity) but the change in the proportion of particles emitted from the thermal source and from independent N-N collisions in the corona.

For each particle type we have

$$\frac{dN(c)}{2\pi p_{\perp} dp_{\perp} dy} = \frac{N_{core}(c)}{2} \frac{dN_{th}}{2\pi p_{\perp} dp_{\perp} dy} + \frac{N_{corona}(c)}{2} \frac{dN_{pp}}{2\pi p_{\perp} dp_{\perp} dy} \quad (2.1)$$

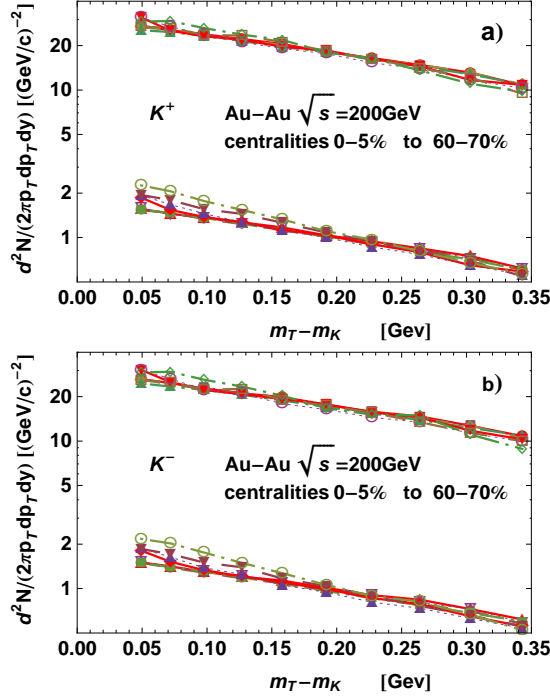


FIG. 1: (Color online) The upper points represent the thermal part of the spectra for  $K^+$  (panel a) and  $K^-$  (panel b) for Au-Au collisions at  $\sqrt{s} = 200\text{GeV}$  (STAR Collaboration data [6]). Spectra are obtained by the fit procedure consisting in subtracting the contribution from the corona and by scaling to the size of the source in 0-5% centrality bin. Results for 8 centrality bins from 0-5% to 60-70% are superimposed. The lower curves represent the raw spectra in different centrality classes divided by the number of participant pairs  $N_{part}/2$  ( $\times 10$ ).

where  $N_{core}(c)$  and  $N_{corona}(c)$  are the number of participants in the core and in the corona at a given centrality  $c$ ,  $dN_{pp}/2\pi p_{\perp} dp_{\perp} dy$  is the spectrum in proton-proton collisions and  $dN_{th}/2\pi p_{\perp} dp_{\perp} dy$  is the spectrum of particles emitted from the thermal fireball per participant pair. The proton-proton spectra  $dN_{pp}/2\pi p_{\perp} dp_{\perp} dy$  have been measured experimentally [6] and can be subtracted from the raw spectra on the left hand side of Eq. (2.1). The thermal spectra  $dN_{core}/2\pi p_{\perp} dp_{\perp} dy$  correspond to particles emitted from the thermal fireball after expansion and freeze-out, we assume that they depend weakly on the centrality. Spectra written below after subtraction and rescaling should not depend on centrality

$$\frac{N_{core}(0-5\%)}{N_{core}(c)} \left[ \frac{dN(c)}{2\pi p_{\perp} dp_{\perp} dy} - \frac{N_{corona}(c)}{2} \frac{dN_{pp}}{2\pi p_{\perp} dp_{\perp} dy} \right]; \quad (2.2)$$

they are equal to the spectra of particles from the thermal fireball in the most central bin (0-5%). For each centrality other than the most central bin Eq. (2.2) represents a constraint on the parameters  $N_{core}$  and  $N_{corona}$ . These parameters should be adjusted to make the spectrum in

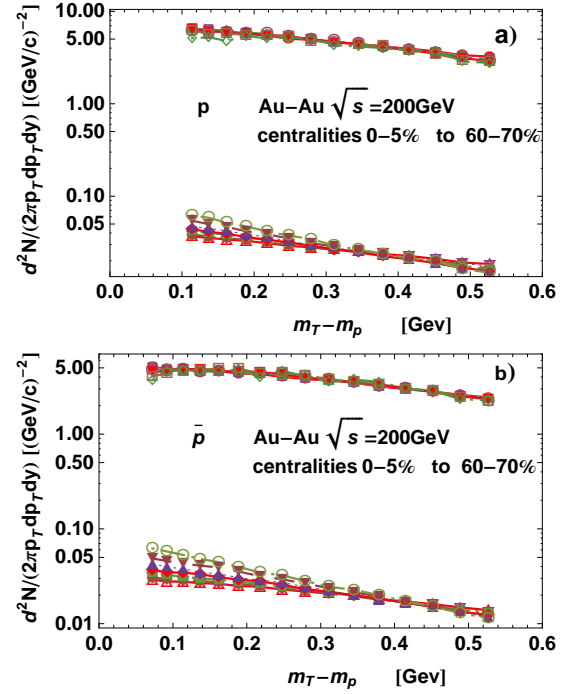


FIG. 2: (Color online) Upper points represent the extracted thermal part of the spectra for protons (panel a) and antiprotons (panel b) similar as for kaons in Fig. 1. Lower points represent the raw measured spectra in different centralities divided by the number of participant pairs  $N_{part}/2$ .

(2.2) as close as possible to

$$\frac{N_{core}(0-5\%)}{2} \frac{dN_{th}}{2\pi p_{\perp} dp_{\perp} dy} = \frac{dN(0-5\%)}{2\pi p_{\perp} dp_{\perp} dy} - \frac{N_{corona}(0-5\%)}{2} \frac{dN_{pp}}{2\pi p_{\perp} dp_{\perp} dy} \quad (2.3)$$

The fit cannot separate the core and corona contributions for one of the centralities, in our case 0-5%. Using the data of the STAR Collaboration [6, 25], for 7 centralities 5-10%, 10-20%, ... to 60-70%, we perform a  $\chi^2$  fit for two parameters  $\alpha(c)$  and  $\beta(c)$  so that the difference between the two sides of the following equation

$$N_{core}(0-5\%) \frac{dN_{th}}{2\pi p_{\perp} dp_{\perp} dy} \simeq \left( \alpha(c) \frac{dN(c)}{2\pi p_{\perp} dp_{\perp} dy} - \beta(c) \frac{dN_{pp}}{2\pi p_{\perp} dp_{\perp} dy} \right) \quad (2.4)$$

is as small as possible. The parameters of the fit are related to  $N_{core}(c)$  and  $N_{corona}(c)$  defining the two-component interaction region

$$\alpha(c) = \frac{N_{core}(0-5\%)}{N_{core}(c)} \quad \beta(c) = \frac{N_{core}(0-5\%)}{2N_{core}(c)} N_{corona}(c) - \frac{N_{corona}(0-5\%)}{2} \quad (2.5)$$

The parameters  $\alpha(c)$  and  $\beta(c)$  are taken the same for 4 kinds of identified particles analyzed  $K^+$ ,  $K^-$ ,  $p$  and  $\bar{p}$ .

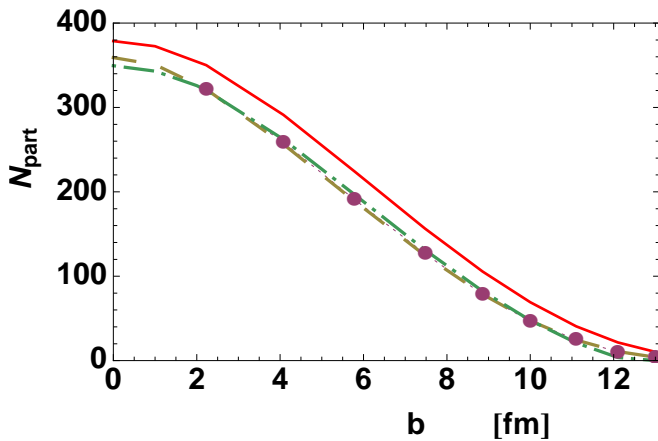


FIG. 3: (Color online) Dependence of the source size on the impact parameter for the Glauber optical model (Eq. 3.4) (solid line), for the thermal fireball defined by the higher density in transverse plane (Eq. 3.5) (dashed-dotted line), and for the thermal fireball defined by nucleons undergoing more than one collision (dashed line). The dots are the results of the fit for the size of the thermal core at different impact parameters.

We did not include pions in the fit. Pions are less sensitive to the transverse flow and their thermal and  $p$ - $p$  spectra are similar. Therefore the fit is not sensitive to the separation between the core and the corona in that case. In Figs. 1 and 2 are shown the spectra transformed according to Eq. (2.4). The procedure of making all spectra look similar after subtraction of the  $p$ - $p$  contribution works moderately well for kaons and very well for protons and antiprotons. The thermal component of the particle emission can be described using one thermal distribution for all centralities. For comparison in the lower part in Figs. 1 and 2 we show the experimental data for different centralities scaled by the number of participating nucleon pairs. It proves that spectra measured for different centralities have different slopes, and after integration would not give the same number of produced kaons, protons or antiprotons per participating pair. Only after subtracting the corona contribution to the spectra a universal thermal emission is recovered.

From the fit, parameters  $N_{core}$  can be extracted for each centrality. The procedure needs an input for  $N_{corona}(0-5\%)$ , we take the value  $N_{corona}(0-5\%) = 29$  suggested by the core-corona models and by the analysis of [21]. The fitted source sizes as function of the impact parameter are shown by the dots in Fig. 3. The thermal fireball size  $N_{core}(c)$  is clearly smaller than the whole interaction region given by  $N_{part}$  from a Glauber model calculation (solid line in Fig.3).

In the Figure are also shown prediction of two models of the core (details of the calculation are presented in the next section.). The first one (dashed-dotted line) is defined by the minimal density of participant nucleons in

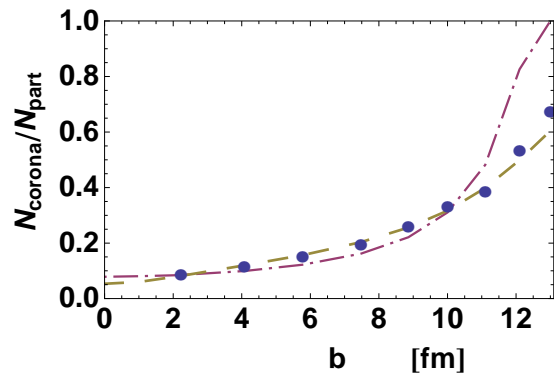


FIG. 4: (Color online) Ratio of the corona size to all participants for the thermal fireball defined by the higher density in transverse plane (Eq. 3.5) (dashed-dotted line), and for the thermal fireball defined by nucleons undergoing more than one collision (dashed line). The dots are the results of the fit for the size of the thermal core at different impact parameters.

the transverse plane  $\rho(x, y) > \rho_{crit}$

$$N_{core} = \int dx dy \rho(x, y) \Theta(\rho(x, y) - \rho_{crit}) . \quad (2.6)$$

The cut-off density is  $\rho_{crit} = 1.2 \text{fm}^{-2}$ . It is smaller than the value  $\rho_{crit} = 2 \text{fm}^{-2}$  used in Ref. [21], but in that previous analysis part of the particles emitted from the corona have been assumed to be absorbed by the core. The dashed line in Fig. 3 represents the core size defined as nucleons that underwent more than one collisions. Counting only the nucleons with  $N_{coll} > 1$  as belonging to the core can explain the strangeness suppression in peripheral collisions [24]. In Fig. 4 is shown the proportion of the core size to the size of the whole interaction region. Both the model based on the minimal density (Glauber model with high density) and the model where the core size is defined by nucleons with multiple collisions (Glauber model with  $N_{coll} > 1$ ) work well for central and semiperipheral collisions  $b < 10 \text{fm}$ . The last model gives correct estimates of the core size also for more peripheral collisions. The two-component analysis of the spectra of identified particles produced at different centralities shows that the emission occurs in two sources within the interaction region. The separation between the two components is somewhat arbitrary. Qualitatively with increasing impact parameter the corona portion of the interaction region increases and the spectra change from thermal like more to N-N collisions like (Fig. 4). We quote two models of the core and corona that give reasonable estimate of their sizes.

### III. DENSE THERMAL SOURCE

The initial distribution of matter in the transverse plane ( $\mathbf{s} = (x, y)$ ) in heavy-ion collisions can be described using the optical Glauber model [26]. Nucleons in the two

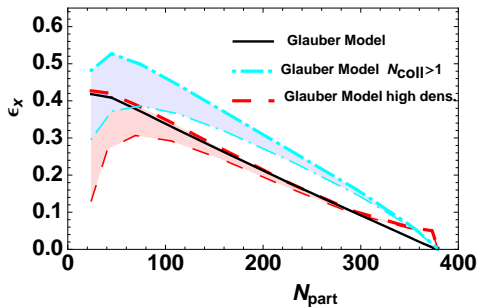


FIG. 5: (Color online) Spatial eccentricity of the initial state from the Glauber model (solid line), from the Glauber model with the density of participants  $> 1.2\text{fm}^{-2}$  (upper dashed line), same but including a weighted contribution of isotropic emission from the corona (lower dashed line), from the Glauber model including only participants with more than one collision (upper dashed-dotted line), same but including a weighted contribution of the isotropic emission from the corona (lower dashed-dotted line).

colliding nuclei are distributed according to the Woods-Saxon density

$$\rho(r) = \frac{\rho_0}{1 + \exp((r - R_A)/a)}. \quad (3.1)$$

For the Au nucleus ( $A = 197$ ) we take [27], the central density  $\rho_0 = 0.161\text{fm}^{-3}$ , the radius  $R_A = 6.5\text{fm}$  and the parameter  $a = 0.535\text{fm}$ . The nuclear thickness function is defined as

$$T_A(\mathbf{s}) = \int_{-\infty}^{\infty} \rho(\sqrt{\mathbf{s}^2 + z^2}) dz. \quad (3.2)$$

For the collision of a symmetric system at impact parameter  $b$ , the density of participants in the transverse plane is

$$\rho_w(\mathbf{s}) = T_A(\mathbf{s} + b/2) \left(1 - \left(1 - \frac{\sigma T_A(\mathbf{s} - b/2)}{A}\right)^A\right) + T_A(\mathbf{s} - b/2) \left(1 - \left(1 - \frac{\sigma T_A(\mathbf{s} + b/2)}{A}\right)^A\right), \quad (3.3)$$

where  $\sigma = 41\text{mb}$  is the N-N cross section. In the optical Glauber model the number of participants is given by

$$N_{part} = \int \mathbf{d}^2\mathbf{s} \rho_w(\mathbf{s}) \quad (3.4)$$

and can be calculated for each impact parameter (solid line in Fig. 3).

In the first model [21] of the dense core, the thermal fireball is restricted to densities above a given minimal density  $\rho_{crit}$

$$\rho_w^{dens}(\mathbf{s}) = \rho_w(\mathbf{s}) \Theta(\rho_w(\mathbf{s}) - \rho_{crit}) \quad (3.5)$$

and the core size as measured by the number of participants is

$$N_{core}^{dens} = \int \mathbf{d}^2\mathbf{s} \rho_w^{dens}(\mathbf{s}). \quad (3.6)$$

$N_w^{dens}$  as function of the impact parameter is shown by the dashed-dotted line in Fig. 3 for  $\rho_{crit} = 1.2\text{fm}^{-2}$ .

The second model [24] of the corona is based on the condition that nucleons undergo more than one collision. The transverse plane density of participants with more than one collision is obtained after a simple calculation

$$\begin{aligned} \rho_w^{coll}(\mathbf{s}) = & T_A(\mathbf{s} + b/2) \left(1 - \left(1 - \frac{\sigma T_A(\mathbf{s} - b/2)}{A}\right)^{A-1}\right. \\ & \left. (1 + \sigma T_A(\mathbf{s} - b/2) \frac{A-1}{A})\right) \\ & + T_A(\mathbf{s} - b/2) \left(1 - \left(1 - \frac{\sigma T_A(\mathbf{s} + b/2)}{A}\right)^{A-1}\right. \\ & \left. (1 + \sigma T_A(\mathbf{s} + b/2) \frac{A-1}{A})\right). \end{aligned} \quad (3.7)$$

The size of the core  $N_{core}^{coll}$  (dashed-dotted line in Fig. 3) is defined analogously to (3.6).

At nonzero impact parameter the interaction region is azimuthally asymmetric. The spatial eccentricity is defined as

$$\epsilon_x = \frac{\int \mathbf{d}^2\mathbf{s} (y^2 - x^2) \rho_w(\mathbf{s})}{\int \mathbf{d}^2\mathbf{s} (x^2 + y^2) \rho_w(\mathbf{s})}. \quad (3.8)$$

The above formula can be used for all three densities of the source defined above  $\rho_w$ ,  $\rho_w^{dens}$  and  $\rho_w^{coll}$ . The results are shown in Fig. 5. This definition of the eccentricity is the so called standard eccentricity [28], that gives zero for head-on collisions. During the expansion, the initial eccentricity is transformed into the momentum eccentricity of the collective flow [29] and eventually into the azimuthal asymmetry of the transverse momentum emission of particles. In the linear approximation, the final elliptic flow coefficient is proportional to  $\epsilon_x$  [30]. This argument should be amended because of the emission from the corona. In the first approximation we assume that the emission from the corona is isotropic. In the experiment, particles from the core (anisotropic emission) and from the corona are summed, this reduces the total anisotropy. On the average the number of particles emitted per participant pair from the core is a factor  $\alpha = 1.65$  larger than from the corona [21]. The weighted eccentricity taking into account the contribution from the corona can be defined as

$$\frac{\alpha N_{core}}{\alpha N_{core} + N_{corona}} \epsilon_x. \quad (3.9)$$

The reduced, weighted eccentricities are shown by the lower dashed and dashed-dotted curves in Fig. 5. The bands between the lower and upper curves in Fig. 5 denote the spread between the core eccentricity and the corresponding weighted eccentricity (3.9). Since some anisotropy in the emission from the corona is possible due to a shadowing effect of the core, we consider the spread in the band as the uncertainty of the prediction of the effective eccentricities.

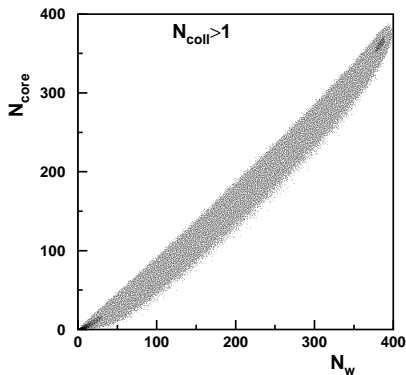


FIG. 6: Histogram of event by event realizations of the number of participants in the core for a fixed number of all participants.

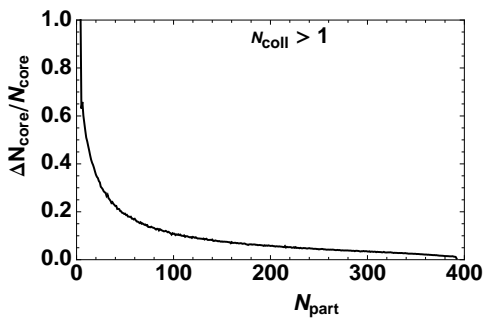


FIG. 7: Scaled standard deviation of the size of the core as function of the number of all participants.

A Monte-Carlo realization of the Glauber model can be used [31]. In the two nuclei the positions of  $A$  nucleons are generated according to the Woods-Saxon distribution (3.1). In the generation of nucleon positions a minimal distance of 0.4fm between two nucleons is imposed. Two nuclei composed of  $A$  nucleons are shifted by  $\pm b/2$  in the  $x$  direction in the transverse plane and straight line trajectories of all the nucleons are followed. A N-N collisions occurs if two nucleons from different nuclei pass within the distance  $\sqrt{\sigma/\pi}$  from each other in the transverse plane. The number of nucleons colliding at least once (all participant nucleons) is recorded, the same for the number of nucleons that collided more than once (nucleons in the core). Their positions in the transverse plane are summed to give the densities  $\rho_w(\mathbf{s})$  and  $\rho_{core}^{coll}(\mathbf{s})$ . Event by event correlation between  $N_{part}$  and  $N_{core}$  is shown in Fig. 6. For more peripheral collisions (and for Cu-Cu collisions) event by event fluctuation of the core size become important (Fig. 7) and could modify the conclusions on the collective flow and final spectra. For smaller impact parameters the relative importance of the fluctuations of the core is smaller and an average of the core size (density) over the events can be used as an initial state of the thermal fireball.

Event by event fluctuations are important for the spatial eccentricity of the initial distribution of collision cen-

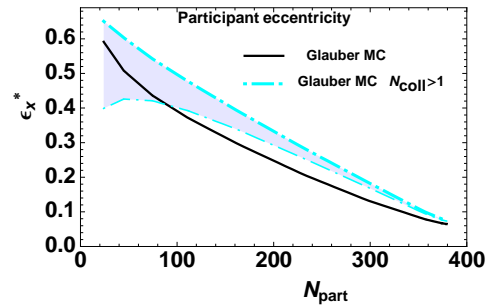


FIG. 8: (color online) Participant eccentricity in the initial state from the Glauber model including event by event eccentricity fluctuations in the distribution of all participants (solid line), of participants with more than one collision (upper dashed-dotted curve), same but including a weighted contribution of the isotropic emission from the corona (lower dashed-dotted line).

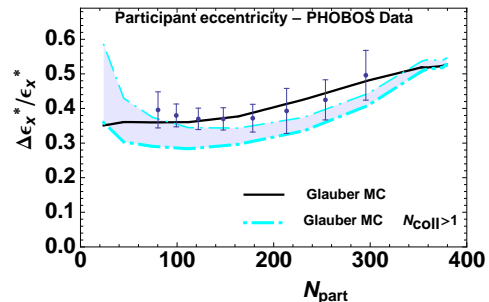


FIG. 9: (Color online) Scaled standard deviation of the participant eccentricity for all participants (solid line), for participants with more than one collision (lower dashed-dotted curve), same but including a weighted contribution of the isotropic emission from the corona (upper dashed-dotted line).

ters in the transverse plane [28, 32]. In each event the coordinates in the transverse plane are rotated to maximize the eccentricity [31]. Even at zero-impact parameter fluctuations of the distribution in the finite number of collision points give non-zero eccentricity. We calculate the eccentricity in this way (the so called participant eccentricity) for the Glauber Monte-Carlo model and for the core defined as nucleons with more than one collision. The eccentricity is larger than in the standard definition (Fig. 8). At zero impact parameter the participant eccentricity is nonzero (and similar) both for all participant nucleons and for nucleons from the core. For intermediate impact parameters, participant eccentricity is larger for participants in the core even after the reduction of the effect by the emission from the corona (Eq. 3.9).

To relate the initial spatial eccentricity to the elliptic flow coefficient  $v_2$  of the observed hadrons a dynamical calculation must be performed. A quantity that is more directly related to the observed particle spectra is the scaled standard deviation of the elliptic flow. The scaled standard deviation in the initial state  $\Delta\epsilon^*/\epsilon^*$  can be compared to measured scaled fluctuations of the ellip-

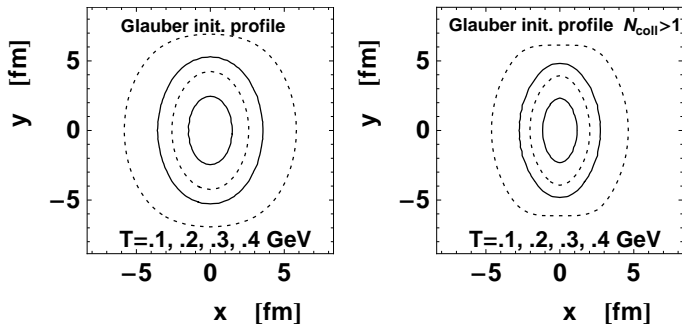


FIG. 10: Contour plot of the initial temperature profile ( $b = 10\text{fm}$ ) when the entropy density is proportional to the participant density from the Glauber model (left panel) or to the density of participants with more than one collision (right panel).

tic flow  $\Delta v_2/v_2$  [33]. Glauber Monte-Carlo model results are very close to the measured scaled elliptic flow coefficient [29, 30, 33] (solid line in Fig. 9). For the core-corona scenario the denominator of the ratio  $\Delta\epsilon^*/\epsilon^*$  is increased, in the numerator we neglect the small contribution from fluctuations of the isotropic corona emission. Thus, the scaled standard deviation is reduced for the core-corona scenario. This reduction is smaller if the weighting (3.9) is applied to the anisotropy of the core. In a more detailed analysis presented in the next section we show that the interplay of the core and corona emission depends on the particle type and the transverse momentum. Since thermal spectra are harder than spectra from N-N emission in the corona, the elliptic flow at intermediate  $p_\perp$  is dominated by the core contribution.

#### IV. HYDRODYNAMIC EXPANSION OF THE THERMAL SOURCE

Matter in the dense fireball created in the first stage of the collision flows in the longitudinal direction. We assume a boost invariant Bjorken scaling expansion in the beam direction. In the transverse direction there is no flow initially, but later, pressure gradients lead to transverse flow and expansion. The expansion can be modelled as ideal fluid hydrodynamics in the dense thermalized phase [13, 14, 15], followed by particle emission at the freeze-out. We solve 2+1-dimensional relativistic hydrodynamic equations

$$\partial_\mu T^{\mu\nu} = 0, \quad (4.1)$$

with the energy-momentum tensor of the form  $T^{\mu\nu} = (\epsilon + p)u^\mu u^\nu - g^{\mu\nu}p$ . With boost-invariance in the longitudinal direction the four velocity is

$$u^\mu = \left( \frac{t}{\sqrt{t^2 - z^2}}\gamma_\perp, v_x\gamma_\perp, v_y\gamma_\perp, \frac{z}{\sqrt{t^2 - z^2}}\gamma_\perp \right), \quad (4.2)$$

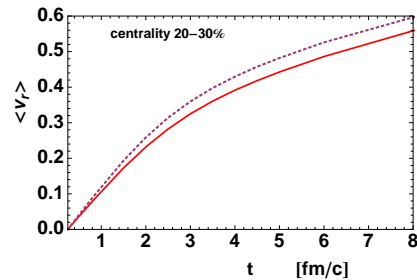


FIG. 11: (Color online) Average transverse velocity (4.4) as function of the time of the hydrodynamic expansion for standard Glauber initial profile (solid line) and for the initial profile including only nucleons with more than one collision (dotted line).

with  $\gamma_\perp = 1/\sqrt{1 - v_x^2 - v_y^2}$ . The energy density  $\epsilon$ , the pressure  $p$  and the velocities  $v_x, v_y$  depend on the transverse coordinates and on the proper time  $\sqrt{t^2 - z^2}$ . Moreover, the energy density and the pressure are related by the EOS. We take a realistic parameterization thereof [34]. The use of such a realistic EOS has been shown to be indispensable for a quantitative description of RHIC measurements [16, 17]. Interpolated lattice data above the critical temperature of  $T_c = 170\text{MeV}$  and an EOS of noninteracting hadrons at lower temperatures are taken. The limiting formulas are joined without a soft point.

We solve numerically hydrodynamic equations for two different initial conditions, the Glauber Model initial density (Eq. 3.5) and the thermal core including nucleons with more than one collision (Eq. 3.7). The entropy density in the fireball created at impact parameter  $b$  is assumed to be proportional to density of participants

$$s(\mathbf{s}, b) = s_0 \frac{\rho_w(\mathbf{s}, b)}{\rho_w(\mathbf{0}, 0)} \quad (4.3)$$

The entropy density  $s_0$  at the center of the fireball in central collisions corresponds to a temperature of 500MeV. For the core scenario we take  $\rho_w^{coll}$  to define the profile of the entropy and the constant  $s_0$  is rescaled to get the same total entropy (for the corona we assume an effective entropy a factor  $1/\alpha$  smaller per participant). Two set of calculations are performed at impact parameters  $b = 2.23, 4.08, 5.78, 7.48, 8.86, 10.0, 11.1, 12.1\text{fm}$  corresponding to centrality bins from 0 – 5% to 60 – 70% [25]. An early initial time of the hydrodynamic evolution is chosen  $\tau_0 = 0.25\text{fm}/c$  [17].

In Fig. 10 is presented a contour plot of the initial temperature for  $b = 10\text{fm}$ . The profile for the dense core is steeper than for the standard Glauber model. Also the eccentricity is larger for nucleons undergoing multiple collisions. Larger gradients of the pressure make the acceleration faster, the average transverse velocity

$$\langle v_r \rangle = \frac{\int dx dy \gamma_\perp v_\perp \epsilon}{\int dx dy \gamma_\perp \epsilon} \quad (4.4)$$

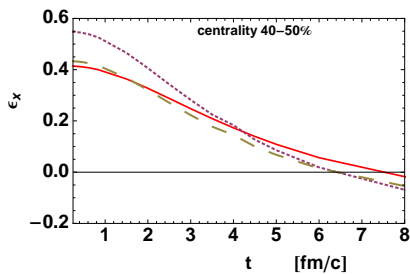


FIG. 12: (color online) Time evolution of the spatial anisotropy (4.5) for the standard Glauber initial profile (solid line), for the initial profile including only nucleons with more than one collision (dotted line), and the same but including a weighted contribution from the isotropic emission from the corona (dashed line).

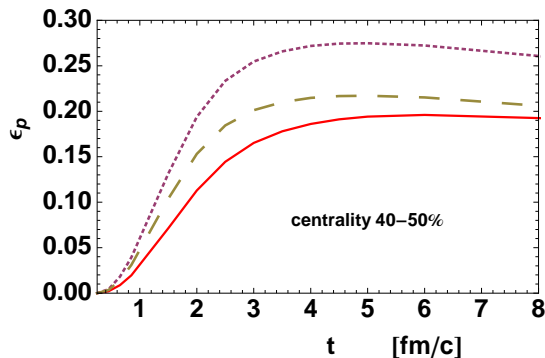


FIG. 13: (Color online) Time evolution of the momentum anisotropy (4.6) for the standard Glauber initial profile (solid line), for the initial profile including only nucleons with more than one collision (dotted line), and the same but including a weighted contribution from the isotropic emission from the corona (dashed line).

increases faster in the expansion of the core (Fig. 11). Spatial eccentricity

$$\epsilon_x = \frac{\int dx dy (y^2 - x^2) \gamma_{\perp} \epsilon}{\int dx dy (x^2 + y^2) \gamma_{\perp} \epsilon} \quad (4.5)$$

decreases during the evolution. The initial eccentricity of the dense core is larger than for the standard Glauber initial density, but faster expansion of the former makes the difference disappear (Fig. 12). If the weighting factor (3.9) is included the effective spatial eccentricity is similar in the two scenarios.

More important for the final particle spectra is the momentum anisotropy

$$\epsilon_p = \frac{\int dx dy (T_{xx} - T_{yy})}{\int dx dy (T_{xx} + T_{yy})}. \quad (4.6)$$

Larger gradients in the in-plane direction cause a stronger collective flow in that direction. Spatial eccentricity disappears, but imprints the velocity field of the fluid (Fig. 13). The momentum anisotropy is stronger if the initial

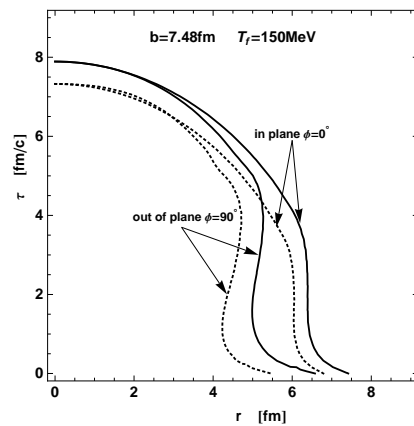


FIG. 14: The freeze-out hypersurface  $T(t, r, \phi) = 150\text{MeV}$  in  $t$ - $r$  coordinates for in plane  $\phi = 0^{\text{deg}}$  and out of plane  $\phi = 90^{\text{deg}}$  directions, for the standard Glauber initial condition (solid lines) and for the initial condition including only nucleons with more than one collision (dashed lines) at impact parameter  $b = 7.48\text{fm}$ .

state is the thermal core, the effect survives the reduction by the weighting factor (3.9).

The hydrodynamic evolution is stopped at the freeze-out temperature  $T_f = 150\text{MeV}$ . The smaller size and larger temperature gradients in the core make it freeze out earlier than the standard fireball composed of all the participant nucleons. Earlier freeze-out means a shorter expansion and less time for the build up of the flow, this partially reduces the effect of faster acceleration in the expansion from the core. From the freeze-out hypersurface  $\Sigma$  particles are emitted according to the Cooper-Frye formula [35]

$$E \frac{dN}{d^3p} = \int_{\Sigma} d\Sigma_{\mu} p^{\mu} f(p^{\mu} u_{\mu}), \quad (4.7)$$

where the integration is over the hypersurface elements  $d\Sigma_{\mu}$  and  $f(p_{\mu} u^{\mu})$  is the thermal (Bose or Fermi) distribution. The procedure of particle emission from the hypersurface and of the decay of resonances is realized using the statistical emission code THERMINATOR [36]. Final  $\pi$ ,  $K$  and  $p$  spectra and the elliptic flow coefficients are calculated.

In Figs. 15 and 16 are shown particle spectra for the two initial densities considered. The spectra are scaled by the number of all participants or by the number of participants in the core respectively. If the initial state is the thermal core, spectra are slightly harder than for the standard Glauber initial conditions. Comparing spectra obtained at different centralities, we notice that the amount of transverse flow is a bit larger for central collisions. This violates to some extent the assumption made in the fit separating the observed spectra into the thermal and direct components (Sect. II). The separation between the core and corona components presented is approximate since the thermal component depends weakly on the centrality of the collision. The elliptic flow coeffi-



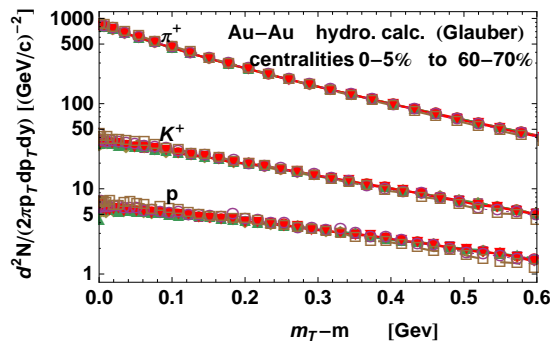


FIG. 15: (Color online) Transverse mass spectra of  $\pi$ ,  $K$  and  $p$  from the hydrodynamic evolution of standard Glauber initial conditions with a freeze-out at  $T_f = 150\text{MeV}$ . Results for 8 centrality classes (0-5%, 5-10%, ..., 60-70%) scaled by the mean number of participant pairs are shown.

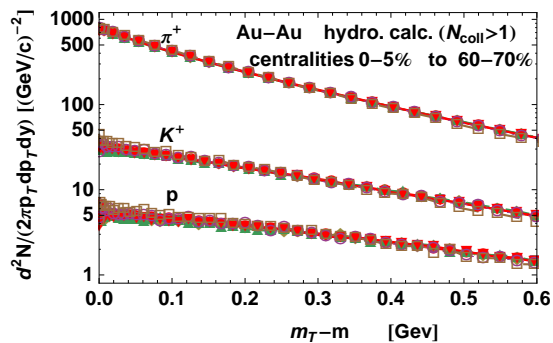


FIG. 16: (Color online) Same as Fig. 15 but for the dense core initial condition ( $N_{coll} > 1$ ).

cient as function of  $p_\perp$  for pions and protons is shown in Figs. 17 and 18. The elliptic flow for particles emitted after the expansion of the core is larger than the elliptic flow calculated for standard Glauber initial conditions. In Sect. III an average reduction factor for the elliptic flow taking into account the emission from the corona is introduced. For the momentum dependent coefficient  $v_2$

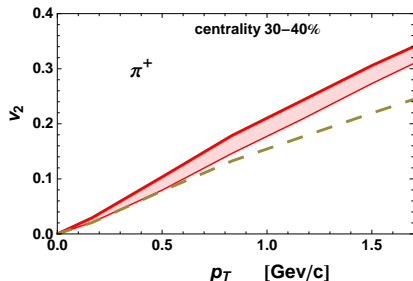


FIG. 17: (Color online) Elliptic flow coefficient  $v_2$  as function of transverse momentum for pions, for the standard Glauber initial condition (dashed line), for the dense core ( $N_{coll} > 1$ ) initial condition (upper solid line) and the same but including the weighted isotropic contribution from the emission from the corona (Eq. 4.8) (lower solid line).

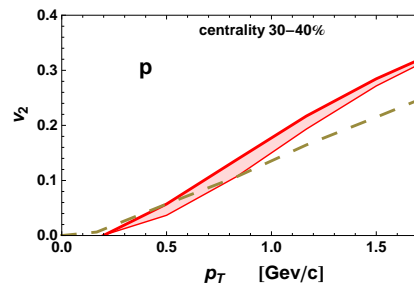


FIG. 18: (Color online) Same as Fig. 17 but for protons.

we use the following reduction factor

$$\frac{N_{core} \frac{dN_{th}}{2\pi p_\perp dp_\perp}}{N_{core} \frac{dN_{th}}{2\pi p_\perp dp_\perp} + N_{corona} \frac{dN_{pp}}{2\pi p_\perp dp_\perp}} v_2(p_\perp). \quad (4.8)$$

The strongest reduction occurs for small momenta. At larger  $p_\perp$  the harder thermal spectra dominate. Thus the difference between the upper solid lines (without the reduction factor (4.8)) and the lower solid lines (with the reduction factor) in Figs. 17 and 18 is small at intermediate  $p_\perp$ . The average reduction factor (3.9) overestimates the effect, especially for heavier particles. The difference between hydrodynamic expansions from the two initial densities is most visible in the final differential elliptic flow in  $p_\perp$ . We expect this effect to be even stronger for smaller colliding systems.

## V. CONCLUSIONS

We discuss the scenario of a two component source in the interaction region in ultrarelativistic nuclear collisions. The interaction region includes a core composed of dense, thermalized matter, that evolves collectively and of an outer corona where particles are emitted in sparse N-N collisions directly. This idea has been proposed earlier in order to explain the increase of particle multiplicity and strangeness content with centrality [21]. In this first estimate the core has been defined as the part of the interaction region with a sufficiently large density of participants. A different definition of the core is proposed in Ref. [24]. Only nucleons that collided more than once emit particles that thermalize. The rest of the participants constitutes the corona. We fit the spectra of kaons, protons and antiprotons at different centralities with two components, a thermal part and a contribution from N-N collisions. The extracted size of the thermal core is compared to the prediction of the two models of the core-corona separation. The size of the core can be defined by the nucleons in the high density region for impact parameters  $b < 10\text{fm}$ , whereas the number of nucleons that underwent several collisions is a good estimate of the size of the thermal core for all centralities.

We give a formula describing the density of nucleons that collided more than once. We calculate the spatial

eccentricity of the models of the dense dense core. For the core composed of nucleons with more than one collisions it is larger than for the standard Glauber model fireball. We expect a strong elliptic flow after the expansion of such a dense, asymmetric core. From a Glauber Monte-Carlo model calculation we find that scaled eccentricity fluctuations are slightly reduced for the emission from the core compared to estimates taking into account all participants [28].

The hydrodynamic evolution starting with the standard Glauber model density of the fireball is compared to the expansion of the core composed of nucleons with multiple collisions. The density of the core has larger gradients and larger spatial eccentricity. It leads to a faster expansion, stronger transverse and elliptic flows. Even

after taking into account the emission from the corona, the final elliptic flow for the core-corona fireball is larger than the one for the standard Glauber model fireball. This result shows that the study the scaling of the elliptic flow with the size of the system should involve also the possibility of a two component emission with proportions changing with centrality.

### Acknowledgments

The author is grateful to Mikołaj Chojnacki for discussions on the hydrodynamic calculations and the freeze-out procedure.

- 
- [1] J. Adams et al. (STAR), Nucl. Phys. **A757**, 102 (2005), nucl-ex/0501009.
  - [2] K. Adcox et al. (PHENIX), Nucl. Phys. **A757**, 184 (2005), nucl-ex/0410003.
  - [3] I. Arsene et al. (BRAHMS), Nucl. Phys. **A757**, 1 (2005), nucl-ex/0410020.
  - [4] B. B. Back et al. (PHOBOS), Nucl. Phys. **A757**, 28 (2005), nucl-ex/0410022.
  - [5] E. Schnedermann, J. Sollfrank, and U. W. Heinz, Phys. Rev. **C48**, 2462 (1993), nucl-th/9307020.
  - [6] J. Adams et al. (STAR), Phys. Rev. Lett. **92**, 112301 (2004), nucl-ex/0310004.
  - [7] A. Andronic, P. Braun-Munzinger, and J. Stachel, Nucl. Phys. **A772**, 167 (2006), nucl-th/0511071.
  - [8] F. Becattini, J. Manninen, and M. Gazdzicki, Phys. Rev. **C73**, 044905 (2006), hep-ph/0511092.
  - [9] J. Cleymans, B. Kampfer, M. Kaneta, S. Wheaton, and N. Xu, Phys. Rev. **C71**, 054901 (2005), hep-ph/0409071.
  - [10] W. Florkowski, W. Broniowski, and M. Michalec, Acta Phys. Polon. **B33**, 761 (2002), nucl-th/0106009.
  - [11] J. Rafelski, J. Letessier, and G. Torrieri, Phys. Rev. **C72**, 024905 (2005), nucl-th/0412072.
  - [12] T. Hirano, N. van der Kolk, and A. Bilandzic (2008), arXiv:0808.2684 [nucl-th].
  - [13] P. Huovinen and P. V. Ruuskanen, Ann. Rev. Nucl. Part. Sci. **56**, 163 (2006), nucl-th/0605008.
  - [14] P. F. Kolb and U. W. Heinz, in *Quark Gluon Plasma 3*, edited by R. Hwa and X. N. Wang (World Scientific, Singapore, 2004), nucl-th/0305084.
  - [15] C. Nonaka, J. Phys. **G34**, S313 (2007), nucl-th/0702082.
  - [16] W. Broniowski, M. Chojnacki, W. Florkowski, and A. Kisiel, Phys. Rev. Lett. **101**, 022301 (2008), arXiv:0801.4361 [nucl-th].
  - [17] M. Chojnacki, W. Florkowski, W. Broniowski, and A. Kisiel, Phys. Rev. **C78**, 014905 (2008), arXiv:0712.0947 [nucl-th].
  - [18] A. Kisiel, W. Broniowski, M. Chojnacki, and W. Florkowski (2008), arXiv:0808.3363 [nucl-th].
  - [19] S. A. Voloshin (STAR), J. Phys. **G34**, S883 (2007), nucl-ex/0701038.
  - [20] Z. Chajeccki and M. Lisa (2008), arXiv:0807.3569 [nucl-th].
  - [21] P. Bozek, Acta Phys. Polon. **B36**, 3071 (2005), nucl-th/0506037.
  - [22] V. S. Pantuev, JETP Lett. **85**, 104 (2007), hep-ph/0506095.
  - [23] K. Werner, Phys. Rev. Lett. **98**, 152301 (2007), 0704.1270.
  - [24] F. Becattini and J. Manninen, J. Phys. **G35**, 104013 (2008), arXiv:0805.0098 [nucl-th].
  - [25] B. Abalev et al. (STAR) (2008), arXiv:0808.2041 [nucl-ex].
  - [26] A. Białas, M. Bleszyński, and W. Czyż, Nucl. Phys. **B111**, 461 (1976).
  - [27] B. I. Abelev et al. (STAR), Phys. Rev. **C75**, 054906 (2007), nucl-ex/0701010.
  - [28] M. Miller and R. Snellings (2003), nucl-ex/0312008.
  - [29] S. A. Voloshin (2006), nucl-th/0606022.
  - [30] W. Broniowski, P. Bozek, and M. Rybczynski, Phys. Rev. **C76**, 054905 (2007), arXiv:0706.4266 [nucl-th].
  - [31] W. Broniowski, M. Rybczynski, and P. Bozek (2007), arXiv:0710.5731 [nucl-th].
  - [32] C. E. Aguiar, Y. Hama, T. Kodama, and T. Osada, Nucl. Phys. **A698**, 639 (2002), hep-ph/0106266.
  - [33] B. Alver et al., Phys. Rev. **C77**, 014906 (2008), 0711.3724.
  - [34] M. Chojnacki and W. Florkowski, Acta Phys. Polon. **B38**, 3249 (2007), nucl-th/0702030.
  - [35] F. Cooper and G. Frye, Phys. Rev. **D10**, 186 (1974).
  - [36] A. Kisiel, T. Taluc, W. Broniowski, and W. Florkowski, Comput. Phys. Commun. **174**, 669 (2006), nucl-th/0504047.